Soil, regolith, and weathered rock: Theoretical concepts and evolution in old-growth temperate forests, Central Europe

Pavel Šamonil[a,b,*], Jonathan Phillips[a,c], Pavel Daněk[a,d], Vojtěch Beneš[e], Lukasz Pawlik[a,f]

[a] Department of Forest Ecology, The Silva Tarouca Research Institute for Landscape and Ornamental Gardening, Lidická 25/27, 602 00 Brno, Czech Republic
[b] Department of Forest Botany, Dendrology and Geobiocoenology, Faculty of Forestry and Wood Technology, Mendel University in Brno, Zemědělská 1, 613 00 Brno, Czech Republic
[c] Earth Surface Systems Program, Department of Geography, University of Kentucky, Lexington, KY 40506, USA
[d] Department of Botany and Zoology, Faculty of Science, Masaryk University, Kotlářská 267/2, 611 37 Brno, Czech Republic
[e] G IMPULS Praha Ltd., Czech Republic
[f] University of Silesia, Faculty of Earth Sciences, ul. Będzińska 60, 41-200 Sosnowiec, Poland

ARTICLE INFO

ABSTRACT

Evolution of weathering profiles (WP) is critical for landscape evolution, soil formation, biogeochemical cycles, and critical zone hydrology and ecology. Weathering profiles often include soil or solum (O, A, E, and B horizons), non-soil regolith (including soil C horizons, saprolite), and weathered rock. Development of these is a function of weathering at the bedrock weathering front to produce weathered rock; weathering at the boundary between regolith and weathered rock to produce saprolite, and pedogenesis to convert non-soil regolith to soil. Relative thicknesses of soil (T_s), non-soil regolith (T_r) and weathered rock (T_w) can provide insight into the relative rates of these processes at some sites with negligible surface removals or deposition. Scenarios of weathering profile development based on these are developed in current study. We investigated these with ground penetrating radar, electrical resistance tomography, and seismic profiling at three old growth forest sites in the Czech Republic, on gneiss, granite, and flysch bedrock.

We found that the geophysical methods – which generated thousands of separate measurements of T_s, T_r, T_w – to produce good estimates. The weathered rock layer (sensu lato) was generally the thickest of the weathering profile layers. Mean soil thicknesses were about 0.64–0.75 m at the three sites, with typical maxima around 1.5 m. Non-soil regolith thicknesses averaged about 2.5 m on the gneiss site and 1.2–1.4 at the other sites. Weathered rock had a mean thickness of 7 m at the gneiss site (up to 10.3), 4.6 at the granite site, and 3.4 on flysch. Results indicate that weathering at the bedrock weathering front is more rapid than conversion of weathered rock to regolith, which is in turn more rapid than saprolite-to-soil conversion by pedogenesis on all three bedrock types. No evidence was found of steady-state soil, non-soil regolith, or weathered rock thicknesses or evolution toward steady-state. Steady-state would require that weathering rates at the bedrock and/or regolith weathering fronts decline to negligible rates as profiles thicken, but the relative thicknesses at our study sites do not indicate this is the case.

1. Introduction

Weathering sets the "metabolic rate" of landscape evolution in many cases. In weathering-limited geomorphic systems denudation rates are directly controlled by the rate at which transportable debris is produced by weathering. In transport-limited systems denudation is limited by transport capacity (Carson and Kirkby, 1972), but the rate at which soils, regolith, and sediment accumulate is ultimately controlled by weathering, though feedbacks exist between denudation, weathering, and accumulation as described below. Weathering processes are numerous, interrelated with each other and numerous other processes (e.g. Merrill, 1906; Goudie and Viles, 2012). Many feedbacks in this complex system in critical zone (Riebe et al., 2017) have been still unknown. It can be argued that the evolution of weathering profiles is one of the most fundamental phenomena in Earth and environmental sciences, being fundamental to the development of soils and the terrestrial biosphere, ecosystem functions, and biogeochemical cycles, as well as a necessary precursor to geomorphic processes (Migoń,

2013a,b). We aim to address the relative rates, importance, and implications of bedrock weathering, regolith accumulation, and pedogenesis. This will be accomplished by examining signatures of these phenomena in weathering profiles from old-growth forests in the Czech Republic, using geophysical data.

We selected old-growth forests because formation of soils and weathering mantles is unaffected by direct human interventions. Non-invasive geophysical techniques were selected to gather a more complete picture of weathering mantles in strictly protected forest reserves. Regolith and soil profiles, and auger and core samples are discrete representations of the weathering mantle continuum. While these point data help to verify spatially continuous geophysical findings, with point data alone we struggle to capture the whole picture of the underground weathering phenomena and their effects: architecture, intensity, magnitude and structural complexity. In many cases this constraint limits full evaluation of the geomorphic and soil system. At least partly, geophysical data help overcome this basic limitation. Further, in many cases, without the use of heavy excavation equipment, pits that include the entire weathering mantle down to bedrock are impossible or impractical.

Beyond their crucial role in landscape and hillslope evolution and models thereof, understanding weathering mantles is also important in a number of practical applications in critical zone. These include hydrology, agriculture, forestry, mineral exploration, geochronology and seismic risk assessment (Wilford and Thomas, 2014). The evolution of weathering mantles is also relevant to the development of layering and stratigraphy, which is crucial in considerations of moisture and pollutant fluxes, carbon storage, and other applications (Lorz et al., 2011) and in palaeoecological and palaeoclimate reconstructions (e.g. August and Wojewoda, 2004; Migoń, 2013a,b). In addition, weathered rock (e.g. flysch, which occurs at one of our study sites) may have soil-like properties, and provide many of the same ecosystem services as soil, including plant substrate, moisture supply, and nutrients; and faunal and microbial habitat (Graham et al., 1994; Stone and Comerford, 1994; Tate, 1995; Wald et al., 2013). The approach here may also be eventually adapted to the study of weathering mantles on extraterrestrial bodies.

2. Terminology

A weathering profile is a vertical section of the weathered mantle from the ground surface to fresh bedrock or other unweathered material in the subsurface. Various terms are used to describe portions of the weathering profile, and some terms are used differently by different authors (see syntheses by Tandarich et al., 2002; Ehlen, 2005; Taylor, 2011; Juilleret et al., 2016). We will not debate terminology here, but given the various terminologies in use, it is important to define our use of various terms.

Bedrock denotes intact, unweathered rock. A bedrock section at the base of a weathering profile (as opposed to bedrock fragments above the weathering front) has ≥ 90 percent intact rock. There may also exist slightly, moderately, or highly weathered rock (see Ollier and Pain, 1996, and Ehlen, 2005 for criteria). In **slightly weathered rock** the rock structure is preserved, microfractures exist, dark minerals start to be altered and on a coarser scale there may be interlocked core stones, including some weathered material. It is potentially slightly calcified, and readily broken with a hammer. **Moderately weathered rock** also conserves rock structure, but has fissures and fractures, and rectangular core stones. Earth material (soil or sediment) is < 50%. It is potentially calcified, and iron or oxide staining may be present; and it can be broken by a kick. Rock structure is still visible in **highly weathered rock**, but core stones are rounded, and unconsolidated material comprises > 50% of the volume. There may exist strong iron or oxide staining and it is potentially strongly calcified and can be broken by hand (Ollier and Pain, 1996; Ehlen, 2005). We use *weathered rock* to refer to slightly and moderately in situ weathered rock including

saprocl below regolith and above bedrock.

Soil is the highly modified (partly by biota) upper portion of a weathering profile and generally encompasses the solum (O, A, E, B horizons, see Schaetzl and Thompson 2015). In this study, soil is considered up to transition between metamorphic B and substratum C horizons. *Regolith* includes the entire weathering mantle above in situ weathered rock, plus any transported material. It thus includes soil, saprolite, and deposited material. The biotic component of weathering is generally reduced here. We use the term *non-soil regolith* to refer to the saprolite and C horizons beneath the solum. We do not consider urban/anthropic or organic soils here.

A *weathering front* is a three dimensional boundary between fresh and weathered rock, which may be a gradual and/or irregular transition zone rather than a sharp separation. Following Phillips et al., 2019, the *bedrock weathering front* is the boundary between fresh bedrock and the overlying weathering mantle at the base of a profile or section. Some profiles may also contain *isolated weathering fronts* associated with core stones or unweathered remnants within a weathering profile. A boundary between moderately and/or slightly weathered rock and overlying regolith we refer to as a *regolith weathering front*.

3. Material and methods

Our general approach is based on linking observations of the depths and thicknesses of soil, regolith, and weathered rock to scenarios of weathering profile development.

3.1. Theory

Let W_1 be the conversion by weathering of fresh bedrock to weathered rock, and W_2 the transformation of weathered rock to saprolite, or non-soil regolith material. P is the formation of soil or solum material from saprolite, etc. The rates of these transformations are dW_1/dt, dW_2/dt, dP/dt, and the amount of transformation over the evolution of the profile ΔW_1, ΔW_2, ΔP. Over some time scales it may appear that rock is converted directly to saprolite, with no intermediate weathered rock stage. We assume that this is not the case; that there is at least a brief intermediate stage. Where there appears to be such a direct transition, this indicates that $dW_2/dt \gg dW_1/dt$.

If $dW_1/dt < dW_2/dt$, then (given sufficient time), weathered rock should be transformed to saprolite quickly relative to the weathering of bedrock, resulting in thinner layers of weathered rock and a relatively sharp weathering front. If $dW_1/dt \approx dW_2/dt$ a significant thickness of moderately to slightly weathered rock would separate regolith from the bedrock interface. Where $dW_1/dt > dW_2/dt$, the weathered rock thickness would increase more rapidly than the regolith thickness.

If $dW_2/dt < dP/dt$, then (given sufficient time), regolith should be transformed to soil quickly relative to the production of regolith, resulting in thinner C, C_r horizons and non-soil regolith, and a relatively sharp transition to weathered rock and/or bedrock. If $dW_2/dt \approx dP/dt$ a significant thickness of regolith would separate the solum from layers containing a large proportion of unweathered bedrock. Where $W_2 > P$, the non-soil regolith thickness would increase more rapidly than solum thickness.

T_s, T_r, T_w represent the thicknesses of soil, non-soil regolith, and weathered rock, respectively. In the absence of subsurface removals that result in reduced thickness or volume (e.g., piping erosion, sapping, dissolution followed by collapse),

$$T_w = \Delta W_1 - \Delta W_2$$
$$T_r = \Delta W_2 - \Delta P$$
$$T_s = \Delta P - \Delta E$$

where ΔE is the net erosion and other mass removal from the surface (with net deposition or addition represented as $-\Delta E$). By definition $\Delta W_1 \geq \Delta W_2 \geq \Delta P$. However, dW_1/dt, dW_2/dt, dP/dt may be quite

variable and are not subject to any analogous constraints.

Although climate, hydrological, and biotic changes, or renewal of exposure by erosion may accelerate weathering, in general weathering and soil formation rates tend to decline over time (Birkeland, 1999; Taylor and Eggleton 2001; Schaetzl and Thompson, 2015). Thickness of soil, regolith, and weathered rock cannot, presumably, increase indefinitely even in the absence of erosion or other surface removals. The soil production function concept indicates that the rate of weathering at the weathering front or base of the regolith declines as the thickness of the overlying soil and regolith increases. In some cases there exists a positive relationship up to some threshold thickness, beyond which the rock weathering rate decreases with additional thickness (often called the humped production function; Humphreys and Wilkinson, 2007). This is presumed to be due to the increasing isolation of the weathering front from meteoric water and biological effects. The production function is supported by several empirical studies (e.g., Dosseto et al., 2008; Stockmann et al., 2014). Pedogenic and bedrock-weathering features such as fragipans, duripans silcretes, and ferricretes might also isolate weathering fronts from percolating water and surficial biological activity.

The weathering-thickness feedbacks described above, and the closely related concept of a steady-state equilibrium regolith thickness, were identified more than a century ago (Davis, 1892; Gilbert, 1909; Penck, 1924). Similarly, pedologists have long recognized that rates of soil formation and changes in pedological properties tend to decline over time, but in that case due to phenomena such as depletion of weatherable minerals and accumulation or compaction of more resistant forms of secondary or residual minerals (e.g. clay minerals or Al-, Fe-oxides and hydroxides, organo-metallic complexes, e.g. Birkeland, 1999; Schaetzl and Thompson, 2015).

To the extent weathering is directly or indirectly dependent on precipitation infiltrated at the surface and biota, a depth limitation is clearly implied. While tree roots and microbes may exist at considerable depths (e.g. Canadell et al., 1996), including in bedrock partings, roots, organic matter, and biological activity decline rapidly below roughly the upper 30 cm of soil. However, locally within a weathering profile, biogenic pathways and hotspots may exist along roots, root paths, tunnels, and burrows well below upper layers.

Fresh rock and a new supply of weatherable minerals are supplied as a weathering front advances, and erosional removals bring fresh rock closer to the surface. Moisture can also be supplied to the weathering front other than via percolation from the surface. Sub-vertical and lateral flows occur in the form of saturated throughflow in the soil, perched water table flows along low-permeability layers, fluxes along bedding planes (or their remnants) and conduit and macropore flow (e.g. Riebe et al., 2017, Phillips et al., 2019). Upward movement occurs at the capillary fringe between the phreatic and vadose zones, and due to water table rise. Upward fluxes also occur due to suction exerted by roots and transpiration by plants, as well as evaporation. Floral and faunal bioturbation can also result in multi-directional mass fluxes (e.g. Schaetzl and Thompson 2015, Román-Sánchez et al., 2019a).

The widespread occurrence of very deep weathering profiles indicates that the decline of weathering rates due to increasing depth of the weathering front is not ubiquitous, and/or that even though weathering declines with depth, it is not always reduced to negligible rates.

Several conceptual frameworks or models in pedology and geomorphology have implications with respect to development of weathering profiles. These are summarized in Table 1, with their implications expressed in terms of the framework described above (review by Pawlik et al., 2016).

Conceptual models of weathering and regolith formation in geomorphology and soil science often implicitly and sometimes explicitly (e.g., Riebe et al., 2017) employ a "conveyor belt" metaphor. As the weathering front advances downward, bedrock is transformed to weathered rock. Toward the surface, weathered rock is transformed to

highly weathered rock or saprolite, and then to soil. This is sometimes simplified to a two- sequence whereby weathering turns bedrock into regolith (or saprolite), and pedogenesis turns regolith into soil (e.g., Gabet and Mudd, 2010; Phillips, 2010; 2018; Eckerer et al., 2016; Riebe et al., 2017)

The soil production function, discussed earlier, implies eventual conversion of weathered material to soil, maintained as a steady-state thickness. The concept of weathering- or transport-limited systems (Carson and Kirkby, 1972), not surprisingly, has different implications for those two cases (Table 1).

The biomantle concept conceives of a surficial layer of soil and regolith actively influenced by floralturbation, faunalturbation, and other biomechanical and biochemical processes (Johnson, 1990; 1993; Johnson et al., 2005). The implications with respect to the weathering profile layers and their evolution depends on the depth of the weathering front relative to the thickness of the biomantle (Table 1). Heimsath and Whipple (2019) linked the strength of parent material, depth of bioturbation, and the soil production function. Román-Sánchez et al. (2019b) used single-grain post-infrared infrared stimulated luminescence to reveal quantitative insights into soil production, bioturbation and erosion–deposition.

Other landscape evolution theories and models assume that weathering at the bedrock weathering front declines with regolith thickness, and sometimes explicitly incorporate the soil production function and weathering vs. transport limitations.

3.2. General scenarios and signatures

As weathering front movement and changes in thickness of weathering profiles can rarely be directly observed, here we define several scenarios, and their manifestations in weathering profile dynamics and morphology. All assume minimal net surface removal or deposition ($\Delta E \approx 0$). The scenarios should not be assumed to encompass all possibilities, even under the assumption of minimal erosion or deposition. Further, environmental changes or internal feedbacks could result in several scenarios occurring over time in the same weathering mantle. At the same time, these scenarios represent testable hypotheses of our research in the Czech old-growth forests, where erosion can reasonably be assumed to be negligible, driven by biomechanical effects of individual trees (Zofin site – Razula site – Phillips et al., 2017, Boubin site – Šamonil et al., 2018a,b). Long-term denudation rates determined using radiometrical data (^{10}Be) reached only 300–400 kg ha^{-1} year^{-1} at the Zofin site (Šamonil et al., 2019, still unpublished radiometrical data from Boubin confirmed general results from Zofin).

- In Scenario 1, W1 declines to a negligible rate, while W2 and P continue. This situation eventually results in a thin or undetectable Tw, as weathered rock is converted to regolith and regolith to soil. The bedrock weathering front becomes static or advances very slowly. The relative thicknesses of soil vs. non-soil regolith thickness are dependent on the relative rates of W2, P.
- Scenario 2 involves W1, W2 both declining to negligible rates, while P continues. This results in minimal Tr, Tw as regolith is converted to soil while rock weathering is negligible. The weathering front and the base of the regolith are static or advance very slowly. Ts increases and attains a steady-state thickness. Eventually soil directly overlies bedrock, or there are only very thin layers of non-soil regolith or weathered rock.
- Scenario 3 occurs where relative rates of W1, W2, P remain proportionally constant. Thus Ts, Tr, Tw all maintain their relative thicknesses. The bedrock weathering front, base of regolith, and base of soil all advance. Relative rates of weathering and pedogenesis are reflected by thickness ratios: Ts/Tr ≈ ΔP/ ΔW2; Tr/Tw ≈ ΔW2/ ΔW1.
- All rates slow down in Scenario 4, but W1 slows more/faster than W2 or P. This scenario is plausible due to depletion of weatherable

Table 1

Conceptual frameworks in geomorphology and pedology and their implications with respect to weathering profiles.

Conceptual model or framework	Implications regarding thickness of weathered layers
Conveyor belt	T_s, T_r, T_{wp} continually and equally thicken or reach steady-state thickness.
Soil production function	T_{wp} maintains steady-state thickness. Pedogenesis gradually converts weathered material to soil, so T_s increases; T_r decreases after steady-state is reached.
Weathering vs. transport-limited systems	If weathering-limited, T_{wp} is small and does not increase. T_s negligible. If transport limited, T_{wp} steadily increases or reaches steady-state.
Biomantle	In shallow weathering mantles, biochemical & biomechanical processes at the weathering front may increase T_{wp}. In thicker mantles, T_s should increase to at least depth of biological activity. Localized, patchy effects may produce local divergence and increased spatial variability.
Early 20th century landscape evolution models (e.g., Davis, Gilbert, Penck, King)	Weathering rate-depth feedbacks similar to soil production function generally assumed, but do not play a definitive role.
Mechanistic hillslope & landscape evolution models	Generally incorporate some version of soil production function and/or weathering & transport-limited concepts.

T_s, T_r, T_{wp} = thickness of soil/solum, non-soil regolith, and entire weathering profile, respectively.

minerals, development of resistant or durable weathering and pedogenic features (e.g. ortstein), and isolation of weathering fronts from the surface due to thickening. Ts, Tr thicken relative to Tw., and the base of the solum and regolith advance slowly. The bedrock weathering front advances even more slowly, or becomes static. Eventually weathering profiles undergoing scenarios 1 and 4 would be difficult or impossible to distinguish based on relative thicknesses alone, though criteria such as weatherable minerals could allow a distinction.

- In Scenario 5 changes in W2, P involve slowing. W1 is unaffected (or the rate decreases more slowly).This is similar to scenario 4, but the bedrock weathering rate is less influenced or unaffected due to continued water inputs to the weathering front. Tw becomes thicker relative to Ts, Tr, and the weathering front advances. The base of the solum and regolith advance more slowly.

- Scenario 6 calls for slowing of P, with W1, W2 either unaffected, or their rates decrease more slowly. This scenario reflects situations where pedogenesis decelerates due to depletion of weatherable minerals, accumulation of resistant features, and deepening of soil to the base of the root zone. W1, W2 are less or unaffected. Soil reaches a static thickness and the base of solum does not advance. The base of the regolith and the weathering front advance. Slow surface erosion due to biogenic creep or other processes (see above) may also stay behind observed slowing soil production.

Based on these scenarios and the theoretical framework outlined earlier, we can link observed properties of the relative thicknesses of soil, non-soil regolith, and weathered rock to possible causes, as shown in Table 2. Only scenario 2 (negligible weathering at the regolith and bedrock weathering fronts, while pedogenesis continues) has an unequivocal signal associated with a single observation in the first column of Table 2, and scenario 2 is also potentially consistent with other observations. This underscores the need to use multiple thickness property criteria and/or other observations to interpret weathered mantles.

Consider a case where soil directly overlies fresh bedrock ($T_s > 0$; T_t, $T_w \approx 0$; $T_s/T_{wp} \approx 1$). These observations are only compatible with scenario 2, and have in fact previously been used as a criterion for steady-state soil thickness (Phillips, 2010). For another example, take a case where there are significant thicknesses of all layers, with relative thicknesses of $T_w > T_s > T_r$. Table 2 shows that only scenario 3 is compatible with all aspects of this situation.

3.3. Study area

The study sites are all on unmanaged old-growth mountain forests in the Czech Republic (Fig. 1). Žofínský Primeval Forest (hereinafter Zofin) has been strictly protected since 1838 and represents the 4th oldest forest reserve in Europe. As far as we know, Boubínský Primeval Forest (hereinafter Boubin) has never been cut and it has been strictly protected since 1858. Forest dynamics in Razula Reserve were weakly affected by selective logging and deadwood haulage till the beginning of the 20th century. The area has been strictly protected since 1933. Long-term spontaneous development of all ecosystems under study allows us to assess naturally developed weathering profiles in three forest landscapes.

Three mountain forest landscapes occur along an altitudinal gradient between 600 and 1108 m a.s.l. on three different bedrock types (Table 3). Haplic Cambisols predominate on flysch in Razula. Primary minerals are altered and secondary (clay) minerals originate in the so called metamorphic B horizon of these comparatively weakly developed soils. Although secondary mineral formation is common also on granite and gneiss (Zofin and Boubin), terrestrial soils in both sites simultaneously express podzolization. Organo-metallic complexes originate jointly with the chemical clay destruction during the podzolization (Entic Podzols) and they are potentially transported downward to illuvial spodic horizons in its advanced stage (Albic Podzols, Sauer et al., 2007). In Zofin, Haplic Cambisols are replaced by slightly podzolized Dystric Cambisols and particularly by Entic Podzols. In higher elevations at Boubin on acidic gneiss, Dystric Cambisols give way to Entic Podzols, which fully predominate, along with a few Albic Podzols. Sharply separated stream valleys and spring areas in all three sites are characteristically covered by Gleysols.

As sites long under forest cover, it can be reasonably assumed that erosion is minimal—certainly there is no recent anthropic erosion, and no evidence of active erosion processes other than in streams (though some evidence of active soil and rock creep and other types of past mass movements does exist, see Phillips et al., 2017; Šamonil et al., 2019). The study sites are also tectonically stable at least through the Quaternary, and as protected areas, any biotic effects on soil and regolith have been minimally directly influenced by humans. Further, previous soil studies indicate that regoliths are composed primarily of in situ weathered material derived from underlying bedrock (Šamonil et al., 2011, 2014). Thus these sites are a near-ideal starting point to study the issues of interest here.

All three studied forest are dominated by beach (*Fagus sylvatica* L.); the proportion of spruce (*Picea abies* (L.) Karsten) increases from Razula through Zofin to Boubin in the highest elevation, where spruce is more competitive. Fir (*Abies alba* Mill) is present but uncommon at all three sites under study. Forest dynamics are driven by fine scale disturbances in these three forested landscapes, with significant influence of infrequent strong disturbance events (storms and bark beetle outbreaks) in Zofin and Boubin (Šamonil et al., 2013). Tree uprooting is currently a key hillslope process at all studied forests (Šamonil et al., 2014, 2018a, Phillips et al., 2017).

3.4. Sampling scheme

The three study reserves were overlain with a rectangular network with a 44.25 m grid spacing (derived from the Czech Forest Inventory network, www.uhul.cz). Geophysical measurements described below

Table 2

Observed realistic weathering mantle thickness properties and possible causes and the scenarios outlined above (WF = weathering front). Black area within triangle represents appearance of individual observation between relative thicknesses of soil (T_s, triangle top), non-soil regolite (T_r, left vertex of triangle), and weathered rock (T_w, right vertex of triangle).

Observation	Graphical expression	Possible causes	Comments	Scenarios
A) $T_{wp} \approx 0$		1. Erosion rate high relative to weathering. 2. Weathering rate very low relative to removal. 3. Recent erosion episode or event. 4. Recent rock exposure.		None without erosion
B) $T_s \approx 0 \ (T_{wp} > 0)$		1. Erosion rate high relative to pedogenesis. 2. Pedogenesis very low relative to removal. 3. Recent erosion episode or event. 4. Recent rock or saprolite exposure.		None without erosion
C) $T_r \approx 0 \ (T_w, T_s > 0)$		1. $dP/dt > dW_2/dt$	Pedogenesis faster than conversion of weathered rock to saprolite	2
D) $T_r, T_w \approx 0 \ (T_s > 0)$		1. $dP/dt > dW_2/dt, dW_1/dt$	Pedogenesis faster than weathering at bedrock or regolith WF	2
E) $T_w \approx 0 \ (T_{wp} > 0)$		1. $dW_2/dt \gg dW_1/dt$ 2. $dW_1/dt \approx 0$	Weathering at regolith WF much faster than at bedrock WF; or bedrock rate is negligible	1, 2, 4
F) $(T_s + T_r)/T_{wp} < 1 \ T_w > 0$		1. $dW_1/dt > 0$	Weathering active at bedrock WF	3, 4, 5, 6
G) $T_s/(T_s + T_r) \approx 1 \ T_r \approx 0$		1. $dP/dt \gg dW_2/dt$ 2. $dW_2/dt \approx 0$	Pedogenesis very rapid compared to weathering or rate at regolith WF negligible	2
H) $T_s/(T_s + T_r) < 1 \ T_r > 0$		1. $dW_2/dt > 0$	Weathering active at regolith WF	1, 3, 4, 5, 6
I) Soil (T_s) thickest layer		1. Deposition or accumulation 2. $dP/dt > dW_1/dt, dW_2/dt$	Rapid pedogenesis and/or slowing of weathering rates under soil cover	1, 2, 4
J) Soil (T_s) thinnest layer		1. Erosional removal 2. $dP/dt < dW_1/dt, dW_2/dt$	Slow pedogenesis and/or acceleration of weathering rates	3, 6
K) Non-soil regolith (T_r) thickest layer		1. Erosional removal & $dW_2/dt > dW_1/dt$ 2. $dW_2/dt > dW_1/dt, dP/dt$	Weathering at regolith WF more rapid than at bedrock WF or pedogenesis	1, 3, 4
L) Non-soil regolith (T_r) thinnest layer		1. $dW_2/dt < dP/dt, dW_1/dt$	More rapid weathering at bedrock WF	2, 3, 5

Table 2 (*continued*)

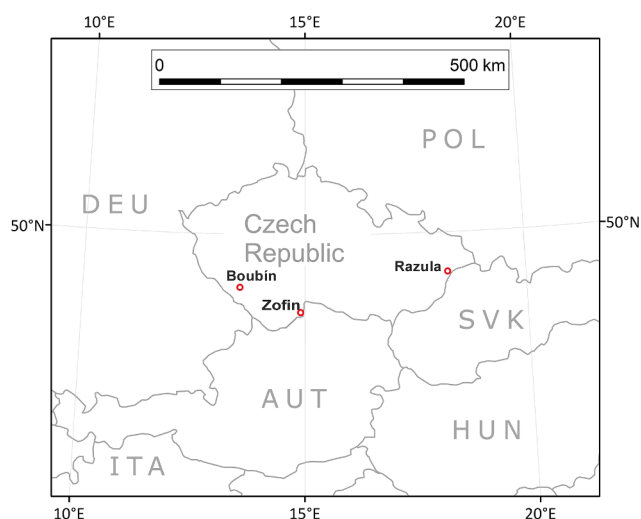| Observation	Graphical expression	Possible causes	Comments	Scenarios
M) Weathered rock (T_w) thickest layer		1. Erosion of soil &/or nonsoil regolith 2. $dW_2/dt > dW_1/dt, dP/dt$	More rapid weathering at bedrock WF	3, 5, 6
N) Weathered rock (T_w) thinnest layer		1. $dW_2/dt, dP/dt \gg dW_1/dt$ 2. $dW_1/dt \approx 0$	Weathering at regolith WF much faster than at bedrock WF; or bedrock rate is negligible	1, 2, 3, 4

Fig. 1. Study sites location map.

were applied in selected rectangles of the network. During the selection, we first excluded incomplete rectangles on edges of the reserves, recently naturally disturbed areas (e.g. windthrow), areas completely covered by natural tree regeneration, or stream and spring areas occupied by hydromorphic soils (Gleysols, Histosols), all inappropriate for geophysical equipment. Geophysical measurement took place in present terrestrial soils along a general gradient of soil weathering and leaching processes. In Razula, where Haplic Cambisols totally predominate, only these soils in two replications of squares

44.25 × 44.25 m were selected for geophysical research. On the other hand, detailed soil maps in Zofin (Šamonil et al., 2011) and Boubin (Daněk et al., 2016) uncovered exceptional local soil diversity. In Zofin four squares about 44.25 × 44.25 m with predominance of Haplic Cambisols, Dystric Cambisols, Entic Podzols, and Albic Podzols were selected. In Boubin, the pattern of soil units was even more complex and selection of relatively homogenous soil units was complicated. That is why we applied geophysical methods on rectangles 44.25 × 22.125 m, in three replications per mapped areas of Dystric Cambisols, Entic Podzols, and Albic Podzols.

Forest reserves have been under intense research on forest dynamics since the 1970 s. At that time positions and dimensions of all standing and lying tree individuals of DBH ≥ 10 cm, their health status (dead standing tree, living tree, dead uprooted tree, breakage etc.), and species was first evaluated within all three reserves (in total 143.7 ha, Průša, 1985). Tree censuses were repeated in the 1990 s and 2000 s in the reserves. Known positions of network nodes (accuracy 0.05 m) fixed in the terrain, as well as exact positions of tens of thousands of trees (accuracy ca 0.5 m) allowed us precise orientation of geophysical measurements in the forests.

3.5. Geophysical methods

Three different geophysical methods were used to determine the position of boundaries between soil, non-soil regolith, weathered rock, and bedrock. At some of the sites, the most distinctive soil horizons were interpreted as well. The advantage of the geophysical methods is their non-destructive nature. For the survey, the following geophysical methods were applied, (i) ground penetrating radar (GPR), (ii) shallow seismic refraction (SSR), and (iii) electrical resistivity tomography (ERT)

Table 3

Main characteristics of the studied sites relevant to environmental conditions, history, and research data.

Feature/Locality	Razula	Zofin	Boubin
Parent material	Flysch	Granite	Gneiss
Taxonomy	Haplic Cambisols	Dystric Cambisols, Entic Podzols, Haplic Gleysols	Entic and Albic Podzols, Haplic and Histic Gleysols
Location (Lat.-Long.) (°)	49°21′35″ N, 18°23′00″ E	48°39′58″ N, 14°42′28″ E	48°58′43″ N, 13°48′43″ E
Average soil reaction (pH_{H2O}) in B-horizon ± SD (n)	5.0 ± 0.2 (14)	4.5 ± 0.2 (13)	4.6 ± 0.2 (21)
Average soil reaction (pH_{KCl}) in B-horizon ± SD (n)	3.6 ± 0.1 (14)	4.1 ± 0.1 (13)	4.0 ± 0.1 (21)
Forest type	fir-beech forest	(spruce)-fir-beech forest	spruce-beech forest
Main tree species	*Fagus sylvatica, Abies alba*	*Fagus sylvatica, Picea abies, Abies alba*	*Fagus sylvatica, Picea abies*
Range of altitudinal gradient (m a.s.l.)	600–812	730–837	925–1108
Mean slope (°)	19.5	8.6	14.4
Mean annual precipitation (mm)	1121	866	1057
Mean average temperature (°C)	6.5	6.2	4.9
Total area of geophysical measurement (ha)	0.4	0.8	0.9
Length of GPR profiles (m)	2100	4100	4800
Length of seismic profiles (m)	180	360	405
Length of thomography profiles (m)	180	0	405

Ground penetrating radar (GPR) was used to consistently identify the lower solum boundary, and the boundary between highly weathered rock (non-soil regolith, saprolite) and moderately or less weathered rock. During the radar measurement, high-frequency electromagnetic waves are emitted into the medium being investigated. Whenever a change in electrical properties of the investigated medium takes place, part of the energy reflects back and is recorded by a receiving antenna. Based on the arrival time of the reflected signal, the depth of the reflecting feature is determined. The travel velocity of the signal through the investigated medium depends mainly on the relative permittivity value. This value was calibrated by comparing the radar records with the description of test pits and ranged from 6 to 10. For the measurement, an antenna of a 400 MHz frequency with adequate resolution and sufficient penetration depth was used. Each selected rectangle of the network was evaluated by GPR in lines 2 m apart. Measurements usually took place in 23 lanes, each 44 m long. Therefore, > 10,000 m was directly evaluated using GPR per all sample plots.

The results of the radar measurements are radar cross-sections showing the record of the electromagnetic wave field reflected off the subsurface materials. Based on the radar cross-sections, the depths of the selected reflective horizons were determined, and spatial coordinates were assigned. Finally, a regular grid of the depths of the interface being interpreted was calculated based on the recorded data and represented as an isopleth map. The reflection intensity of the signal at the investigated interface, corresponding to the physical contrast between the individual layers, was monitored as well. The reflection intensity is affected by many parameters, such as changes in electrical resistivity values, particle size and water saturation. Thickness of soil (T_s) and if possible also thickness of non-soil regolith (T_r) were validated by excavation of deep soil profiles by hand as deep as possible (up to 1.8–3.5 m, Fig. 2). Positions of layers visible in GPR were identified in excavated profiles described using standard pedomorphic methods (Schoeneberger et al., 1998). For deeper evaluation we used soil corers (diameters 3 and 6 cm) in the bottom of excavated profiles.

Shallow seismic refraction (SSR) is based on the elastic signal travelling through a medium between the shot point (impact of the seismic hammer) and recording point (geophone at the profile). The refracted wave is produced at the interface between the slower and faster medium. In our case, this is the interface between the regolith (soils and weathered rock) and the bedrock. Based on the dependence of the seismic signal arrival time and the distance from shot point (the so-called travel-time curve), the shape of the refraction interface may be determined along with the seismic velocities in the overburden and underlying layers. Seismic velocity is a parameter usable for a description of the geomechanical rock properties. Higher seismic velocity values indicate firmer/more compacted rocks/soils.

For the measurement, the geophones were laid out along a selected two GPR profiles per square one profile per lower rectangular plot (Boubin Reserve) at a 1 m spacing. The hammer strokes were situated at every 6th geophone. For the velocity model construction, the principle of tomography was used. The model is presented in the form of a velocity cross-section with the interpreted refraction interface plotted in. The t0 method was used to calculate the depths of the refraction interfaces and the corresponding boundary velocity values (Gurvič, 1975).

Electrical resistivity tomography (ERT) is a direct-current electrical method. It works by measuring resistivity values of soils and rock using **a great** number of electrodes placed along a profile. The electrodes at the profile are interconnected by a special cable that enables progressive connecting of the electrodes as current or potential ones. This allows measuring **a great** number of variants of a 4-electrode array with differing geometry (distance of the current electrodes) resulting in a different depth of penetration.

The method was applied in the same profiles where GPR and SSR took place. The electrode spacing along the profile was 1 m. Measurements were made using a Schlumberger electrode array with a maximum distance of the current electrodes being 30 m. The survey output is an inverted resistivity model of the medium below the profile, represented as a 2D resistivity cross-section. The variation in resistivity values depends on the lithologic composition of the medium and water saturation. Higher resistivity values indicate dry or coarse-grained/firm medium (sands, rubble, firm rock), whereas lower resistivity values correspond to increased moisture content or a fine-grained/disturbed medium (silts, clays, fractured rock).
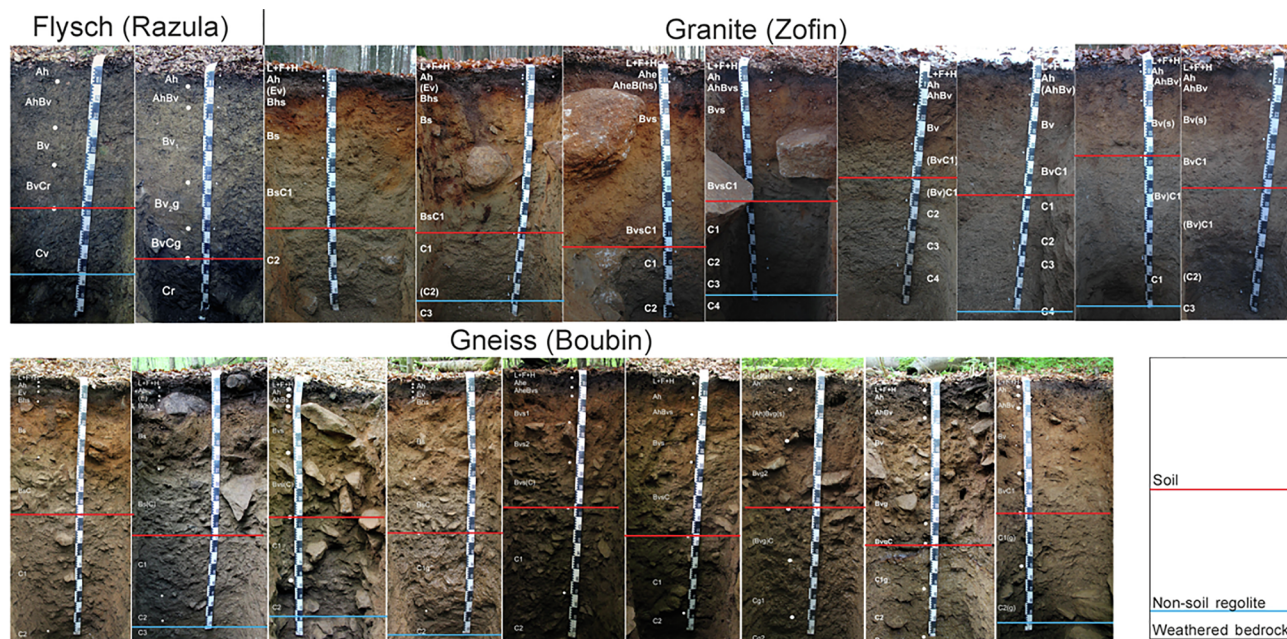

Fig. 2. Soil profiles within three temperate old-growth forests. Abbreviations and borders of individual soil horizons as well as soil depth and non-soil regolite bottom are expressed by red and blue lines. (For interpretation of the references to colour in this figure legend, the reader is referred to the web version of this article.)

3.6. Data processing and analysis

The differences in layer thickness between localities were tested using linear mixed-effects models (function lme from the nlme package, Pinheiro et al., 2018) with individual profiles taken as random effects and spatial autocorrelation along the profiles accounted for by an exponential correlation structure. Function glht from the multcomp package (Hothorn et al., 2008) was then used for Tukey's post hoc testing. All analyses were performed in R (R Core Team, 2018).

4. Results

4.1. Accuracy of weathering layers detection by geophysical approach

Visual evaluation of soil thickness (T_s) within all 19 excavated deep profiles was crucial for spatial determination of T_s using GPR record in all three localities. Position of non-soil regolite was visually verified in 60% of cases on face of excavated profile or on profile by soil borer from the bottom on deep profiles. On granite (Zofin) and flysch (Razula) two layers having the highest reflectance corresponded well with the target positions T_s and T_r (Fig. 2). On gneiss (Boubin) GPR overestimated thickness of soil (T_s). The most reflective threshold occurred between the first and second soil substratum horizon (C1 vs. C2), and genetic soil depth above was only weakly visible. Although soil thickness was not visible everywhere in Boubin, we finally obtained this information on majority of area using GPR in this locality. In some individual cases in all three localities, transition between clear B horizon (spodic or cambic) and transitional substratum horizon including weak soil aggregates (BC) was more reflective than deeper found transition between BC and clear substratum (C) horizon. Adjacent information from continual or neighboring profiles helped us to distinguish between them.

Tomography (ERT) and seismic (SSR) approach helped us to verify validity of T_s and T_r, and were crucial in detection of the deepest T_w (Fig. 3). Unfortunately, we were not able to verify position of this layer in weathering profile visually because of excessive deepness, solidity of material, and destructive approach in forest reserves. However, relationship between studied geophysical properties (e.g. seismic rates in material of various type and weathering degree) are well known (e.g. Samouëlian et al., 2005). Ability of GPR to detect T_w was limited due to decreasing spatial accuracy along depth profile.

4.2. Thickness of soil, non-soil regolith, and the bedrock

Thicknesses of three evaluated layers within the weathering profiles (T_s, T_r, T_w) on three different geological bedrock types were quite variable in depth and thickness (Figs. 4–9). However inner-site variability did not overlay inter-site variability. Average thickness of each layer on gneiss (Boubin) differed significantly from two other bedrock types and localities (ANOVA with Tukey's post hoc test, $p < 0.001$). Soil and non-soil regolite differed significantly between flysch region (Razula) and the granite (Zofin, $p = 0.018$, 0.001 respectively), thickness of weathered bedrock was not statistically different between them ($p = 0.170$).

Mean thickness of soil was the lowest on gneiss (Boubin, 0.64 m), middle on flysch (Razula 0.72 m) and the largest on granite (Zofin, 0.75 m). Maximum soil depth was much higher, it was around 1.5 m in all three localities. The minimal soil depth was between 0.27 and 0.41 m. Variability of soil thickness was lowest on flysch in Razula, where standard deviation (SD) of the soil thickness was only 0.10 m. SD in Zofin and Boubin was 0.16 m and 0.13 m, respectively.

Thickness of non-soil regolith significantly exceeded thickness of soil solum, especially on gneiss (Boubin), where the non-soil regolith thickness was at average 2.51 m and maximal thickness reached 3.95 m. These numbers were significantly lower on flysch (Razula) as well as on granite (Zofin), where mean values were 1.2 m and 1.37 m, respectively. Variability in thickness was lowest in Razula (SD = 0.12) and the largest in Boubin (SD = 0.37 m).

The thickness of weathered bedrock reached 10.3 m in Boubin; the local mean was 7.0 m. We found the uppermost position of the bedrock in Razula, where mean thickness of the weathered bedrock reached 3.41 m. On granite (Zofin) the mean weathered bedrock thickness was 4.6 m. As usual, variability was lowest on flysch, i.e. Razula site.

4.3. Observations and scenarios

Relative proportions of three evaluated layers, T_s, T_r, and T_w, clearly show general predominance of T_w in all three forest reserves in the Czech Republic (Fig. 6). Greater thicknesses of T_w compared to soil is even more visible on gneiss (Boubin) and especially in expression in absolute thicknesses (Figs. 7 and 8). Soil usually represents the thinnest evaluated layer followed by non-soil regolith. On flysch (Razula) the thicknesses of these two layers, T_s, and T_r, were frequently balanced.

From viewpoint of the hypothetical observations defined in Table 2, the actual observations most frequently correspond to observation F and M, where the weathered rock is thicker than soil and non-soil regolith (Figs. 6 and 9). These are associated with active weathering at the bedrock weathering front (WF) and/or more rapid rates of bedrock weathering than of conversion of weathered rock to regolith or regolith to soil. Soil is simultaneously thinner than non-soil regolite (observation H) clearly suggesting progress weathering active in regolite – WF. Some of the weathering profiles can locally correspond with observations I, J, K, L. Case L is also associated with active weathering at the bedrock WF. Particularly on gneiss, but occasionally also on other bedrock types, soil represented thinnest layer in weathering profile (observation J), most probably due to slow pedogenesis and/or active hillslope processes (including local lateral soil extraction by tree uprooting events). On the other hand, soil represented rarely thickest layer (observation I). Sporadic occurrence of the thickest non-soil regolite in weathering profiles (observation K) suggests active weathering in this zone. Missing types of observation represent an erosively active area (observations A, B), or, conversely, steady-state soil behavior.

With respect to the six potential scenarios outlined earlier, observations suggest scenarios 3, 5, and 6 are most common in our forest reserves. This suggests active weathering process in bedrock and potential soil denudation, especially on gneiss (Boubin).

5. Discussion

5.1. Geophysical techniques

Samouëlian et al. (2005) reviewed application of different ERT methods in soils science and Parsekian et al. (2014) reviewed various geophysical techniques used in research of the main critical zone layers formation. Parsekian et al (2014) concluded that the best quality results were acquired when at least two geophysical methods were applied jointly. In a granite massif in north-west Spain, coinciding low velocity refraction and resistivity values indicated the highest weathering class with an opposite pattern for the lowest weathering class (Olona et al., 2010). In our study we appreciated integration of results of GPR, SSR, and ERT, especially in detection of the deepest layer of weathered bedrock. In case of shallower layers detection combination of excavated profiles with GPR were key in the Czech old-growth forests.

The depth of target layer below the surface as well as physical properties of evaluated material are crucial in success and the precision of their detection. In New Caledonia, Robineau et al. (2007) were able
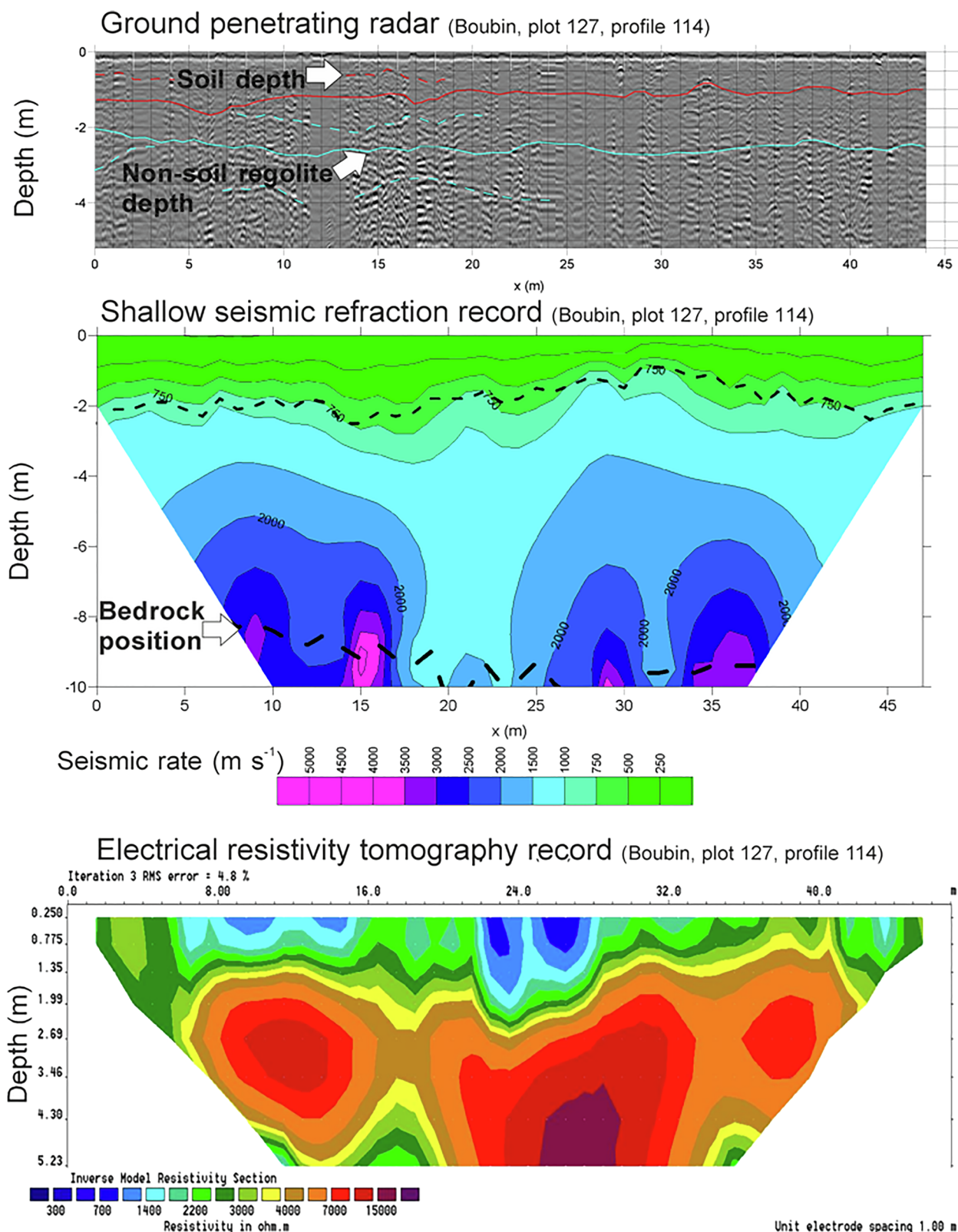
Fig. 3. Example of shallow seismic refraction and electrical resistivity tomography records (Boubin Reserve, plot no. 127, profile 114, gneiss).

to identify well-defined geoelectrical layers with resistivity contrasts down to 100 m (e.g. fine saprolite, coarse saprolite and bedrock, see also Beauvais et al., 1999). In contrast, shallow resistivity mapping of soil layer allowed a precise delineation of hardpan distribution and the changes in clay content (Tabbagh et al., 2000).

5.2. Thickness of weathered rock

In assessments of weathering mantle thickness or depth to bedrock, the thickness of moderately and slightly weathered rock is often overlooked. For practical considerations (e.g., ability to excavate,
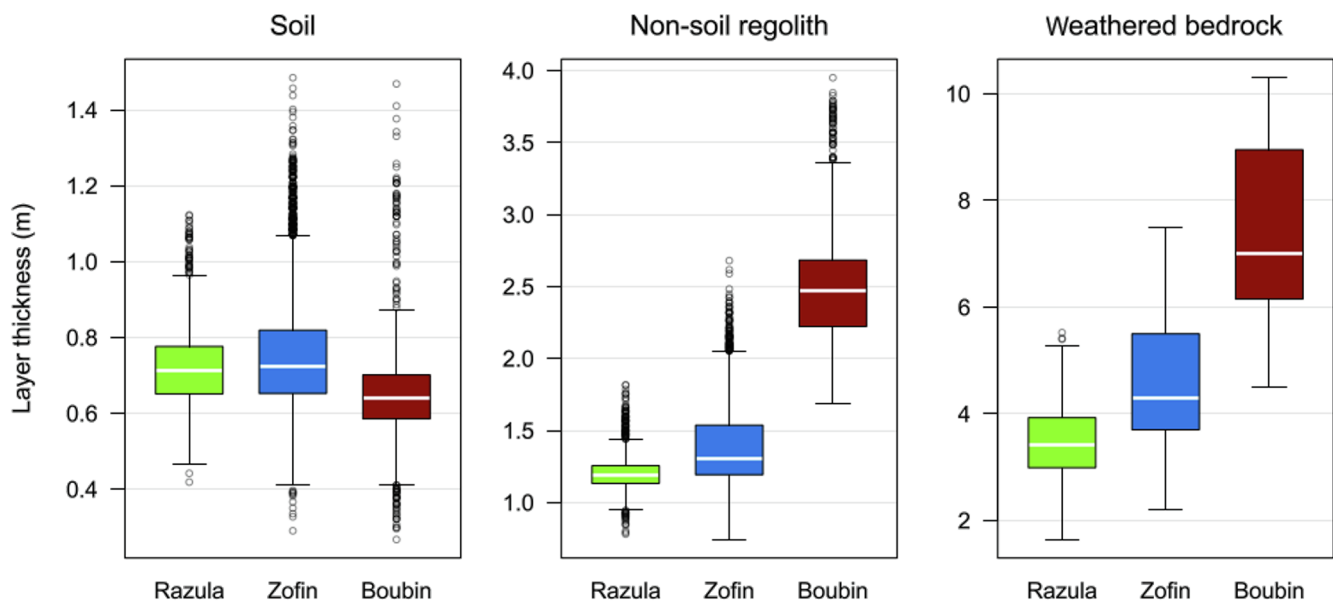
Fig. 4. Box-plots of the layers T_s, T_r, T_w in three old-growth forests in the Czech Republic.

engineering purposes) depth to bedrock is commonly taken as depth to the top of; moderately weathered rock at the base of highly weathered rock or saprolite (Ehlen, 2005). This is probably also the case for many soil profile descriptions that record an R (bedrock) horizon (Phillips et al., 2019). Results of this study support the suggestion of Phillips et al. (2019) that in situ weathered rock may be relatively common, and of significant thickness, with the implication that depth to unweathered bedrock may be underestimated in many cases. The weathered rock layer at our sites was significantly thick on every transect and almost every individual measurement, and was generally the thickest of the weathering profile layers.

5.3. Thickness of soil

Differences in soil thicknesses between sites and bedrock types were statistically highly significant despite their relatively small differences, due to the large data set including thousands of evaluated weathering profiles per site. Soil was thickest in Zofín, where we expect lowest denudation rates (Šamonil et al., 2019). High local variability in soil thickness in all three localities is likely associated with lateral (i.e. sideways) movement of soil (most often in direction of slope inclination) and localized effects on thickness due to tree uprooting. Soil thickness variations are not correlated with variations in surface topography, and the substantial thickness of non-soil regolith and weathered rock make it unlikely that parent material variation has significant effects on soil thickness. While some faunalturbation occurs, tree uprooting and biomechanical effects of trees are ubiquitous, and have been shown to be related to soil morphology at these sites (Samonil et al., 2014, 2015; 2018a,b; Phillips et al., 2017; Pawlik and Šamonil, 2018). In addition, root wads of large uprooted trees often include saprolite and rock fragments, showing that the uprooting directly influences thickness.

5.4. Rates of weathering and pedogenesis

As we do not have age control, we are unable to estimate absolute rates of weathering and soil formation. However, the geophysical data do allow assessment of the relative rates of weathering with respect to alteration of intact parent rock to weathered rock (W1), conversion of

weathered rock to non-soil regolith (particularly saprolite; W2), and formation of soil (P). In the aggregate, our results suggest that weathering at the bedrock WF is the most rapid of these (even if we count the slope denudation effect, see Šamonil et al., 2019). This may indicate the importance of groundwater, as discussed in the next section, and the relatively rapid exploitation of structural weaknesses such as joints and fractures and localized areas of low strength or resistance to chemical weathering. Once initiated, positive feedbacks may allow relatively swift transition to a moderately weathered state (Royne et al., 2008; Worthington et al., 2016; Brantley et al., 2017).

Radiometric dating of soils and rock outcrops at all three sites suggests ages of weathering profiles on the order of tens to hundreds of thousands of years (Šamonil et al., 2019). Thus the WPs have undergone Quaternary climate and ecological changes that affected weathering and pedogenesis rates and observed thicknesses of soil, non-soil regolith, and weathered bedrock. For example, it is likely that weathering proceeded slowly during the last ice age in the generally unglaciated Czech area, while intensified soil erosion may have inhibited soil formation during that time (e.g. Schachtman et al., 2019). Šamonil et al. (2019) noted slightly increasing soil erosion during the transition from glacial to postglacial periods in Zofin as well. The profiles have thus developed under varying, nonlinear rates of weathering and soil formation.

The thickness of non-soil regolith is generally greater than that of soil at our study sites. Locally, this may indicate some surface removal by erosion including biogenous creep (Pawlik and Šamonil, 2018), in particular tree uprooting (Šamonil et al., 2018a), However, in general the sites are not significantly affected by soil erosion (Phillips et al., 2017; Šamonil et al., 2019). This therefore suggests that, at least in terms of thickness, alteration of weathered rock to saprolite exceeds the rate of saprolite-to-soil conversion by pedogenesis on all three bedrock types; granite, gneiss, and flysch. There exist several possible reasons for this. One is the slowing of chemical weathering and clay neoformation rates due to depletion of weatherable minerals. Second is that pedologically important biological activity such as bioturbation, litter inputs, organic acid formation, and soil respiration decline rapidly with depth. Similarly, translocation processes associated with downward-percolating water may decrease with depth. Thus, as soils reach a thickness whereby biological activity and/or vertical translocation are
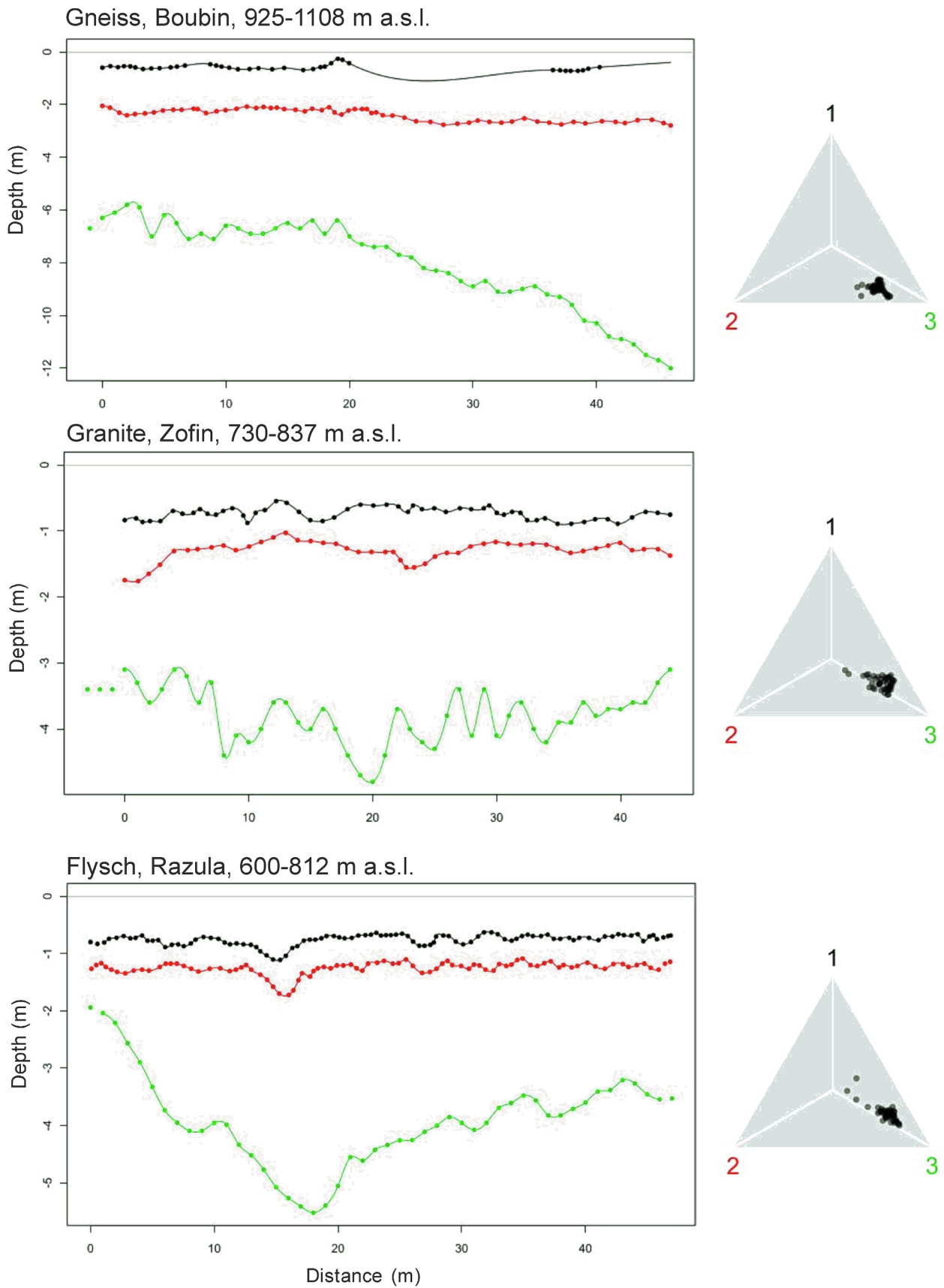
Fig. 5. Examples of weathering profiles structure in three old-growth forests in the Czech Republic and relative proportion of thicknesses of evaluated layers (T_s, T_r, T_w) within the triangle graph. Individual points on curves show positions of depths evaluation, these were interpolated by spline model (curves). Parts of profile of low T_s reflectance in Boubin are represented by black solid line without any points.
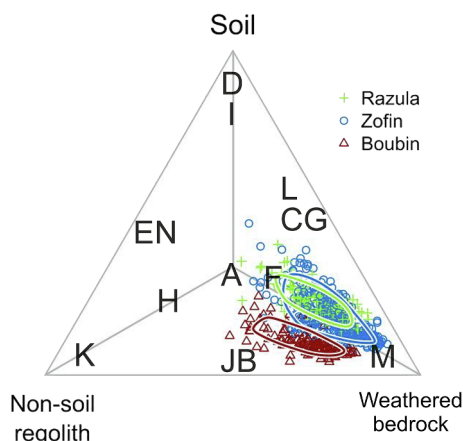
Fig. 6. Relative proportion of thicknesses of three evaluated layers of weathering profiles on gneiss (Boubin Reserve, triangles), granite (Zofin Reserve, circles), and on flysch (Razula Reserve, crosses); only profiles having complete information about all three layers are included. Polygons include 95% of cases within individual localities. The letters represent approximate position of hypothetical observation according to Table 2.

reduced, their rate of growth (downward extension) declines. Additionally, intense podzolization associated with formation of organo-metallic complexes, their illuviation and precipitation in deeper soil horizons, may limit soil deepening. It could play a role on gneiss and granite, where Podzols predominate and where the biggest difference between soil thickness and deeper horizons exist.

5.5. Non-steady-state weathering profiles

Results from three sites with contrasting geology show no evidence of (an approach to) steady-state thicknesses of soil, non-soil regolith, or weathered rock. This would require that weathering rates at the bedrock and/or regolith weathering fronts decline to negligible rates as profiles thicken (i.e., as soil and regolith accumulate). Observations of the relative thicknesses of soil, non-soil regolith, and weathered rock at our study sites do not suggest that this is the case. Rather, in all three lithologies weathering at the bedrock WF is active, and in most cases appears to exceed the rates of regolith and soil formation in the past.

The logic behind the soil production function and steady-state thickness is that weathering processes are driven mainly by inputs of precipitation at the surface, and biological activity concentrated in a surficial biomantle (Humphreys and Wilkinson, 2007). If this is the case, then increasing isolation of weathering fronts from this ground-surface-concentrated activity should indeed result in a decline in weathering rates underneath thicker soil and regolith layers. Our results clearly suggest significant weathering rates even in cases of thick weathered bedrock and the regolith.

We attribute this non-steady-state and active weathering at WFs in some cases 10 m below the surface to effects of groundwater within fractured bedrock and at the bedrock WF, and biological effects, especially tree roots. Even though biological activity and coarse root mass is concentrated in the upper meter of the regolith, vegetation facilitates infiltration of excess moisture, and flow along roots and root channels allows percolation to pass through soil to deeper layers. We have also observed in the field root penetration well into weathered rock, where biomechanical, biochemical, and hydrological affects all stimulate subsurface weathering.

All the study profiles are well above the level of local stream incision. This local base level appears to set the base level (approximate maximum depth) of weathering profiles in many cases, and is directly associated with groundwater drainage (Linton, 1955; Ford and Williams, 2007; Goodfellow et al., 2014; Rempe and Dietrich, 2014; Harman and Cosans 2019). Riebe et al. (2017) hypothesized that
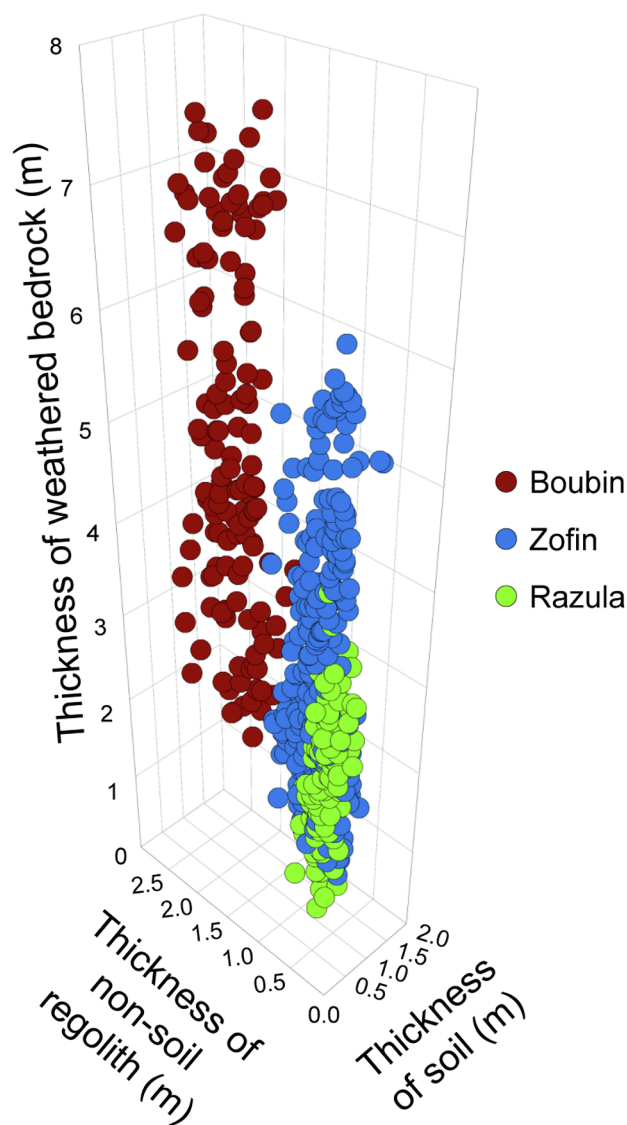

Fig. 7. Absolute thicknesses (m) of studied T_s, T_r, and T_w layers in weathering profiles on gneiss (Boubin Reserve, brown circles), granite (Zofin Reserve, blue circles), and on flysch (Razula Reserve, green circles); only profiles having complete information about all three layers are included. Polygons include 95% of cases within individual localities. (For interpretation of the references to colour in this figure legend, the reader is referred to the web version of this article.)

drainage of chemically-equilibrated groundwater initiates (or rejuvenates) weathering at the weathering front. The recognition of biological activity and moisture as the weathering driving factors clearly indicates the seasonality of non-soil regolite and soil formation (e.g. Schaettzl and Rothstein, 2016). However, our data do not allow to study short-term dynamics of the weathering profile formation.

5.6. Parent material controls

While all three sites show the same general trends and relative thicknesses of the soil, non-soil regolith and weathered bedrock (T_w, T_r and T_s), Figs. 4–8 show that with respect to absolute thicknesses, the sites represent three distinct populations. This is attributed primarily to different parent materials. In general, weathering profiles are deepest on gneiss, shallowest on flysch, and intermediate on granite. This shows the importance of parent material control, as differences in climate, biological communities, and topography are less pronounced. However,
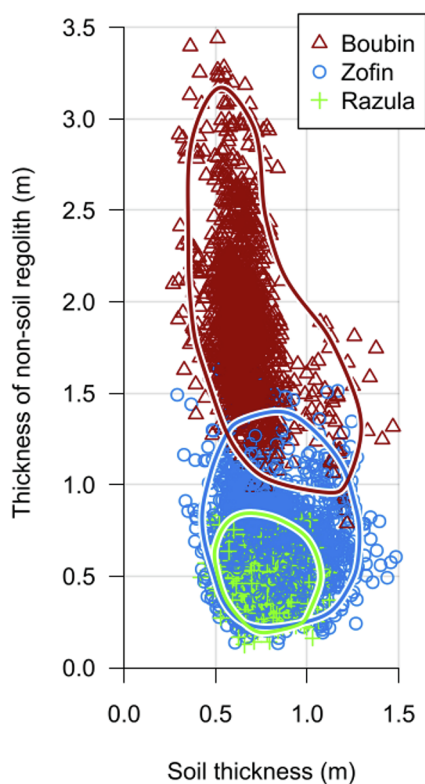
Fig.8. Thicknesses of T_s and T_r layers on gneiss (Boubin Reserve, brown triangles), granite (Zofin Reserve, blue circles), and on flysch (Razula Reserve, green crosses); all profiles are included. Site-specific packing curves are expresses. (For interpretation of the references to colour in this figure legend, the reader is referred to the web version of this article.)

current climate change and associated changes in composition of biological communities and disturbance regimes of the ecosystems (e.g. Seidl et al., 2014) may lead to changes in weathering rates.

We did not expect the flysch site (Razula) to show the thinnest weathering profiles. The parent rock formations contain layers of shales that are (as is often the case with shale) physically weak and with low resistance to chemical weathering. Further, the rocks here are tilted allowing moisture and plant roots to penetrate along bedding planes.

6. Summary and conclusions

The evolution of weathering profiles sets the metabolic rate for landscape evolution, and is critical with respect to soil formation, biogeochemical cycling, and critical zone hydrology and ecology. While
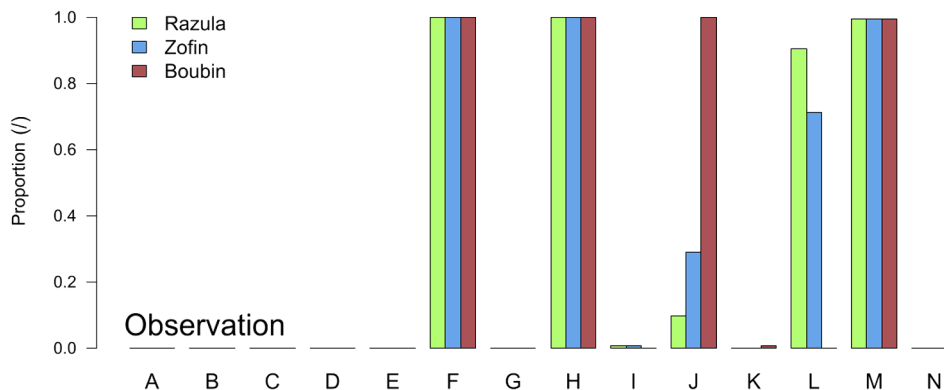
weathered mantles or "soil" is sometimes considered as a single unconsolidated layer above intact bedrock. Weathering profiles actually typically include at least three distinct layers–soil or solum (O, A, E, and B horizons), non-soil regolith (including C horizons, saprolite), and weathered rock. The development of these layers can be considered as a function of three processes–weathering at the bedrock weathering front to produce weathered rock; weathering at the regolith weathering front (boundary between regolith and weathered rock) to produce saprolite, and pedogenesis to convert non-soil regolith to soil. The relative thicknesses of soil (T_s), non-soil regolith (T_r) and weathered rock (T_w) can provide insight into the relative rates of these processes in some settings where surface removals or deposition is minimal via signatures and scenarios of relative thicknesses.

However, one problem with such investigations is practical issues associated with observation and data collection, especially in thicker weathering profiles. We sought to overcome these difficulties with a suite of geophysical measurements: ground penetrating radar, electrical resistance tomography, and seismic profiling. The techniques were applied at three non-eroding old growth forest sites in the Czech Republic, on gneiss, granite, and flysch bedrock. We found that the geophysical methods–which generated thousands separate measurements of T_s, T_r, T_w–to produce good estimates.

Results of this study indicate that T_w layers of significant thickness may be relatively common, with the implication that depth to unweathered bedrock may be underestimated in many cases. The weathered rock layer at our sites was significantly thick on every transect and almost every individual measurement, and was generally the thickest of the weathering profile layers. Mean soil thicknesses were about 0.64 to 0.75 m at the three sites, with typical maxima around 1.5 m. Non-soil regolith thicknesses averaged about 2.5 m on the gneiss site and 1.2 to 1.4 at the other sites. Weathered rock had a mean thickness of 7 m at the gneiss site (up to 10.3), 4.6 at the granite site, and 3.4 on flysch. Local variability in soil thickness in all three localities is likely associated primarily with lateral movement of soil and localized effects on thickness due to tree uprooting.

Results indicate that weathering at the bedrock WF is more rapid than conversion of weathered rock to regolith, which is in turn more rapid than saprolite-to-soil conversion by pedogenesis on all three bedrock types. No evidence was found of steady-state soil, non-soil regolith, or weathered rock thicknesses or evolution toward steady-state. Steady-state would require that weathering rates at the bedrock and/or regolith weathering fronts decline to negligible rates as profiles thicken, but the relative thicknesses at our study sites do not indicate this is the case.

The data came exclusively from old-growth forests. In other words, we avoided past direct human interventions during the site selection. Extending this research to anthropogenically changed or even formed ecosystems may allow to study the role of human in landscape formation.

Fig. 9. Proportions of observed weathering mantle thicknesses that correspond to the possible observations defined in Table 2. We consider the thickness of a layer to be close to zero (TX ≈ 0) if it is lower than 1/10 of the mean thickness of the layer across all localities.

Declaration of Competing Interest

The authors declare that they have no known competing financial interests or personal relationships that could have appeared to influence the work reported in this paper.

Acknowledgement

Appendix A. Supplementary data

Supplementary data to this article can be found online at https://doi.org/10.1016/j.geoderma.2020.114261.

References

August, C., Wojewoda, J., 2004. Late Carboniferous weathering and regolith at the Kudowa Trough, West Sudetes: palaeogeographic, palaeoclimatic and structural implications. Geologia Sudetica 36, 53–66.

Beauvais, A., Ritz, M., Parisot, J.-C., Dukhan, M., 1999. Analysis of poorly stratified lateritic terrains overlying a granitic bedrock in West Africa, using 2-D electrical resistivity tomography. Earth Planet. Sci. Lett. 173, 413–424.

Birkeland, P., 1999. Soils and geomorphology. Oxford University Press. Third edition. pp. 448.

Brantley, S.L., Eissenstat, D.M., Marshall, J.A., Godsey, S.E., Balogh-Brunstad, Z., Karwan, D.L., Papuga, S.A., Roering, J.J., Dawson, T.E., Evaristo, J., Chadwick, O., McDonnell, J.J., Weathers, K.C., 2017. Reviews and syntheses: on the roles trees play in building and plumbing the Critical Zone. Biogeosci. Discuss. doi: 10.5194/bg-2017-61.

Canadell, J., Jackson, R.B., Ehleringer, J.R., Mooney, H.A., Sala, O.E., Schulze, E.D., 1996. Maximum rooting depth of vegetation types at the global scale. Oecologia 108, 583–595.

Carson, M.A., Kirkby, M.J., 1972. Hillslope form and process. Cambridge University Press, pp. 475.

Daněk, P., Šamonil, P., Phillips, J.D., 2016. Geomorphic controls of soil spatial complexity in a primeval mountain forest in the Czech Republic. Geomorphology 273, 280–291.

Davis, W.M., 1892. The convex profile of badland divides. Science 20, 245.

Dosseto, A., Turner, S.P., Chappell, J., 2008. The evolution of weathering profiles through time: new insights from unanium-series isotopes. Earth Planet. Sci. Lett. 274, 359–371.

Eckerer, J., Chabaux, F., Van der Woerd, J., Viville, D., Pelt, E., Kali, E., Lerouge, C., Ackerer, P., Roupert, R.D., di, C., Negrel, P., 2016. Regolith evolution on the millennial timescale from combined U-Th-Ra isotopes and in situ cosmogenic Be-10 analysis in a weathering profile (Strengbach catchment, France). Earth Planet. Sci. Lett. 453, 33–43.

Ehlen, J., 2005. Above the weathering front: contrasting approaches to the study and classification of weathered mantles. Geomorphology 67, 7–21.

Ford, D.C., Williams, P.W., 2007. Karst Hydrology and Geomorphology. John Wiley & Sons: Chichester. pp. 562.

Gabet, E., Mudd, S., 2010. Bedrock erosion by root fracture and tree throw: a coupled biogeomorphic model to explore the humped soil production function and the persistence of hillslope soils. J. Geophys. Res. 115F4, 1–14.

Gilbert, G.K., 1909. The convexity of hilltops. J. Geol. 17, 344–350.

Goodfellow, B.W., Chadwick, O.A., Hilley, G.E., 2014. Depth and character of rock weathering across a basaltic-hosted climosequence on Hawai'i. Earth Surf. Proc. Land. 39, 381–398.

Goudie, A.S., Viles, H.A., 2012. Weathering and the global carbon cycle: Geomorphological perspectives. Earth Sci. Rev. 113, 59–71.

Graham, R.C., Tice, K.R., Guertal, W.R., 1994. The pedologic nature of weathered rock. Whole Regolith Pedology. Soil Science Society of America special pub, Madison, WI, pp. 21–40.

Gurvič, I. I. 1975. Seismorazvedka, Moskva, Nedra.

Harman, J.C., Cosans, C.L., 2019. A low-dimensional model of bedrock weathering and lateral flow coevolution in hillslopes: 2. Controls on weathering and permeability profiles, drainage hydraulics, and solute export pathways. Hydrol. Process. 33, 1168–1190.

Heimsath, A.M., Whipple, K.X., 2019. Strength matters: resisting erosion across upland landscapes. Earth Surf. Proc. Land. 44, 1748–1754.

Hothorn, T., Bretz, F., Westfall, P., 2008. Simultaneous Inference in General Parametric Models. Biomet. J. 50, 346–363.

Humphreys, G.S., Wilkinson, M.T., 2007. The soil production function: a brief history and its rediscovery. Geoderma 139, 73–78.

Johnson, D.L., 1990. Biomantle evolution and the redistribution of earth materials and artifacts. Soil Sci. 149, 84–102.

Johnson, D.L., 1993. Dynamic denudation evolution of tropical, subtropical and temperate landscapes with three-tiered soils: toward a general theory of landscape evolution. Quat. Int. 17, 67–78.

Johnson, D.L., Domier, J.E.J., Johnson, D.N., 2005. Reflections on the nature of soil and its biomantle. Ann. Associat. Am. Geograph. 95, 11–31.

Juilleret, J., Dondeyne, S., Vancampenhout, K., Deckers, J., Hissler, C., 2016. Mind the gap: a classification system for integrating the subsolum into soil surveys. Geoderma 264, 332–339.

Linton, D.L., 1955. The problem of tors. Geogr. J. 121, 470–487.

Lorz, C., Heller, K., Kleber, A., 2011. Stratification of the regolith-continuum – a key parameter for landscape properties. Zeitschrift für Geomorphologie 55 (3), 277–292.

Merrill, G.P., 1906. A Treatise on Rocks, Rock-Weathering and Soils. The MacMillian Company, New York.

Migoń, P., 2013a. Weathering mantles and long-term landform evolution. In: John F. Schroder (ed.), Treatise on Geomorphology, Vol. 4, San Diego: Academic Press, pp. 127–144.

Migoń, P., 2103b. Weathering and hillslope development. In: John F. Schroder (ed.), Treatise on Geomorphology, Vol. 4, San Diego: Academic Press, pp. 159–178.

Ollier, C., Pain, C., 1996. Regolith, Soils, and Landforms. Chichester, U.K. John Wiley.

Olona, J., Pulgar, J.A., Fernández-Viejo, G., López- Fernández, C., González-Cortina, J.M., 2010. Weathering variations in a granitic massif and related geotechnical properties through seismic and electrical resistivity methods. Near Surf. Geophys. 8, 585–599.

Parsekian, A.D., Singha, K., Minsley, B.J., Holbrook, W.S., Slater, L., 2014. Multiscale geophysical imaging of the critical zone. Rev. Geophys. 53, 1–26.

Pawlik, L., Phillips, J., Šamonil, P., 2016. Roots, rock, and regolith: biomechanical and biochemical weathering by trees and its impact on hillslopes – a critical literature review. Earth-Sci. Rev. 159, 142–159.

Pawlik, L., Šamonil, P., 2018. Soil creep: the driving factors, evidence and significance for biogeomorphic and pedogenic domains and systems – a critical literature review. Earth Sci. Rev. 178, 257–278.

Penck, W., 1924. Morphological Analysis of Landforms. English translation by Czech, H., Boswell, K.C., 1953. London, Macmillan.

Phillips, J.D., Šamonil, P., Pawlik, L., Trochta, J., Daněk, P., 2017. Domination of Hillslope Denudation by Tree Uprooting in an Old-Growth Forest. Geomorphology 276, 27–36.

Phillips, J.D., 2010. The convenient fiction of steady-state soil thickness. Geoderma 156, 389–398.

Phillips, J.D., 2018. Self-limited biogeomorphic ecosystem engineering in epikarst. Phys. Geogr. 39, 304–328.

Phillips, J.D., Pawlik, L., Šamonil, P., 2019. Weathering fronts. Earth Sci. Rev. https://doi.org/10.1016/j.earscirev.2019.102925.

Pinheiro, J., Bates, D., DebRoy, S., Sarkar, D., R Core Team, 2018. nlme: Linear and Nonlinear Mixed Effects Models. R package version 3.1-137, URL: https://CRAN.R-project.org/package=nlme.

Průša, E., 1985. Die böhmischen und mährischen Urwälder—ihre Struktur und Ökologie, Vegetace ČSSR A15. Academia, Praha.

R Core Team, 2018. R: A language and environment for statistical computing. R Foundation for Statistical Computing, Vienna, Austria. URL: https://www.R-project.org/.

Rempe, D.M., Dietrich, W.E., 2014. A bottom-up control on fresh-bedrock topography under landscapes. Proceed. Natl. Acad. Sci. (USA) 111, 6576–6581.

Riebe, C.S., Hahm, W.J., Brantley, S.L., 2017. Controls on deep critical zone architecture: a historical review and four testable hypotheses. Earth Surf. Proc. Land. 42, 128–156.

Robineau, B., Join, J.L., Beauvais, A., Parisot, J.-C., Savin, C., 2007. Geoelectrical imaging of a thick regolith developed on ultramafic rocks: groundwater influence. Aust. J. Earth Sci. 54, 773–781.

Román-Sánchez, A., Reimann, T., Wallinga, J., Vanwalleghem, T., 2019a. Bioturbation and erosion rates along the soil-hillslope conveyor belt, part 1: insights from single-grain feldspar luminescence. Earth Surf. Proc. Land. 44, 2051–2065.

Román-Sánchez, A., Laguna, A., Reimann, T., Giráldez, J.V., Peña, A., Vanwalleghem, T., 2019b. Bioturbation and erosion rates along the soil–hillslope conveyor belt, part 2: quantification using an analytical solution of the diffusion–advection equation. Earth Surf. Proc. Land. 44, 2066–2080.

Royne, A., Jamtveit, B., Mathiesen, J., Malthe-Sorenssen, A., 2008. Controls on rock weathering rates by reaction-induced hierarchical fracturing. Earth Planet. Sci. Lett. 275, 364–369.

Šamonil, P., Daněk, P., Schaetzl, R.J., Tejnecký, V., Drábek, O., 2018a. Converse pathways of soil evolution caused by tree uprooting: a synthesis from three regions with varying soil formation processes. Catena 161, 122–136.

Šamonil, P., Daněk, P., Schaetzl, R.J., Vašíčková, I., Valtera, M., 2015. Soil mixing and evolution as affected by tree uprooting in three temperate forests. Eur. J. Soil Sci. 66, 589–603.

Šamonil, P., Daněk, P., Senecká, A., Adam, D., Phillips, J.D., 2018b. The biomechanical effects of trees in a temperate forest. Earth Surf. Proc. Land. 43, 1063–1072.

Šamonil, P., Doleželová, P., Vašíčková, I., Adam, D., Valtera, M., Král, K., Janík, D., Šebková, B., 2013. Individual-based approach to the detection of disturbance history through spatial scales in a natural beech-dominated forest. J. Veg. Sci. 24, 1167–1184.

Šamonil, P., Egli, M., Steinert, T., Abiven, S., Norton, K., Daněk, P., Brandová, D., Christl, M., Hort, L., Tikhomirov D., 2019. Soil denudation rates in an old-growth mountain temperate forest driven by tree uprooting dynamics, Central Europe. Land Degradation and Development. doi: 10.1002/ldr.3443.

Šamonil, P., Valtera, M., Bek, S., Šebková, B., Vrška, T., Houška, J., 2011. Soil variability through spatial scales in a permanently disturbed natural spruce-fir-beech forest. Eur. J. Forest Res. 130, 1075–1091.

Šamonil, P., Vašíčková, I., Daněk, P., Janík, D., Adam, D., 2014. Disturbances can control fine-scale pedodiversity in old-growth forest: Is the soil evolution theory disturbed as well? Biogeosciences 11, 5889–5905.

Samouëlian, A., Cousin, I., Tabbagh, A., Bruand, A., Richard, G., 2005. Electrical

resistivity survey in soil science: a review. Soil Tillage Res. 83, 173–193.

Sauer, D., Sponagel, H., Sommer, M., Giani, L., Jahn, R., Stahr, K., 2007. Podzol: Soil of the year 2007. A review on its genesis, occurrence, and functions. J. Soil Sci. Plant Nutrit. 170, 581–597.

Schachtman, N.S., Roering, J.J., Marshall, J., Gavin, D.G., Granger, D.E., 2019. The interplay between physical and chemical erosion over glacial-interglacial cycles. Geology 47, 613–616.

Schaettzl, R.J., Rothstein, D.E., 2016. Temporal variation in the strength of podzolization as indicated by lysimeter data. Geoderma 282, 26–36.

Schaetzl, R.J., Thompson, M.I. 2015. Soils – Genesis and Geomorphology. 2nd ed. Cambridge University Press, pp. 795.

Schoeneberger, P.J., Wysicki, D.A., Benham, E.C., Broderson,W.D., 1998. Field Book for Describing and Sampling Soils. Natural Resources Conservation Service, USDA, National Soil Survey Center, Lincoln, NE.

Seidl, R., Schelhaas, M.-J., Rammer, W., Verkerk, P.J., 2014. Increasing forest disturbances in Europe and their impact on carbon storage. Nat. Clim. Change 4, 806–810.

Stockmann, U., Minasny, B., McBratney, A.B., 2014. How fast does soil grow? Geoderma 216, 48–61.

Stone, E.L., Comerford, N.B., 1994. Plant and animal activity below the solum. Whole

Regolith Pedology: Soil Science Society of America Special Publication, vol. 34, Madison, WI, pp. 57–74.

Tabbagh, A., Dabas, M., Hesse, A., Panissod, C., 2000. Soil resistivity: a non-invasive tool to map soil structure horizobation. Geoderma 97, 393–404.

Tandarich, J.P., Darmody, R.G., Follmer, L.R., Johnson, D.L., 2002. Historical development of soil and weathering profile concepts from Europe to the United States of America. Soil Sci. Soc. Am. J. 66, 335–346.

Tate, R.L., 1995. Soil Microbiology. John Wiley & Sons, Inc, pp. 398.

Taylor, G., 2011. The evolution of regolith. In: Gregory, K.J., Goudie, A.S. (Eds.), Handbook of Geomorphology. Sage, London, pp. 281–290.

Taylor, G., Eggleton, R.A., 2001. Regolith geology and geomorphology. John Willey & Sons.

Wald, J.A., Graham, R.C., Schoeneberger, P.J., 2013. Distribution and properties of soft weathered bedrock at < 1 m depth in the contiguous United States. Earth Surf. Proc. Land. 38, 614–626.

Wilford, J., Thomas, M., 2014. Predicting regolith thickness in the complex weathering setting of the central Mt Lofty Ranges, South Australia. Geoderma 206, 1–13.

Worthington, S.R.H., Davies, G.J., Calvin Alexander Jr., E., 2016. Enhancement of bedrock permeability by weathering. Earth Sci. Rev. 160, 188–202.